This article has been accepted for publication in a future issue of this journal, but has not been fully edited. Content may change prior to final publication. Citation information: DOI 10.1109/JLT.2021.3066479, Journal of Lightwave Technology

Ultra-compact optical switches using slow light bimodal silicon waveguides

Luis Torrijos-Morán, Antoine Brimont, Amadeu Griol, Pablo Sanchis, *Senior Member, IEEE* and Jaime García-Rupérez, *Senior Member, IEEE*

***Abstract*—Switches are essential components in several optical applications, in which reduced footprints are highly desirable for mass production of densely integrated circuits at low cost. However, most conventional solutions rely on making long switching structures, thus increasing the final device size. Here, we propose and experimentally demonstrate an ultra-compact 2x2 optical switch based on slow-light-enhanced bimodal interferometry in one-dimensional silicon photonic crystals. By properly designing the band structure, the device exhibits a large group index contrast between the fundamental even mode and a higher order odd mode for TE polarization. Thereby, highly dispersive and broadband bimodal regions for high-performance operation are engineered by exploiting the different symmetry of the modes. Two configurations are considered in the experiments to analyze the dimensions influence on the switching efficiency. As a result, a photonic switch based on a bimodal single-channel interferometer with a footprint of only 63 μm^2, a power consumption of 19.5 mW and a crosstalk of 15 dB is demonstrated for thermo-optic tunability.**

***Index Terms*—Optical switch, bimodal waveguide, slow light, silicon photonics.**

I. Introduction

SWITCHES play a prominent role in current communication networks to address the ever-growing increase in the data centers traffic [1]. In this context, photonics offers remarkable advantages in terms of low power consumption and high speed operation for switching applications [2], [3]. Switching light is usually accomplished by interference between signals that have propagated along different optical paths. To this end, the most common photonic structures employed are ring resonators and Mach-Zehnder interferometers (MZIs). Resonant schemes allow very small footprints but at expenses of decreasing the optical bandwidth [4], [5]. In turn, MZI switches offer a broader bandwidth as well as a higher tolerance to fabrication deviations, although long optical paths that increase the resulting footprint are required [6]–[8]. Optical switches based on multimode interferometers (MMIs) exhibit both a broadband operation and robustness [9]. However, these types of structures suffer from a higher power consumption, thus requiring further improvement in the heaters geometry and fabrication to design short devices [10].

On the other hand, ultra-compact phase shifters are possible by integrating materials with unique optical properties in silicon. Transparent conducting oxides, such as Indium Tin Oxide (ITO), have been used either as a more efficient heater [11] or in hybrid photonic waveguide as an active material [12]–[14]. In the latter, phase shifter lengths in the micrometer range have been demonstrated but with high insertion losses. Thereby, the replacement of ITO by high-mobility transparent conducting oxides such as cadmium oxide have been proposed to reduce optical losses [15], [16]. Alternatively, photonic crystals (PhCs) have also been largely investigated for thermo-optic switching with ultra-compact lengths and low power consumption [17]. PhCs allow to drastically reduce the group velocity of the propagating mode, the so-called slow light phenomenon, thus increasing the optical length interaction while the physical length remains small [18]–[20]. This effect is exploited, for instance, to develop 2D hole patterned array PhC structures for all-optical switching based on high speed MZIs [21], or for thermo-optic effects in high-performance MMIs [22] and ultra-compact directional couplers of less than 100 μm^2 footprint [23], [24]. 2D PhCs configurations have also been used to develop optical microcavities for extremely low consumption at the sub-femtojoule level [25]. However, decreasing the group velocity also makes light coupling to the PhC modes to be more inefficient and reduces the optical bandwidth, which must be addressed when using slow light structures [26].

Due to its structural complexity, including 2D PhCs adds extra difficulties in micro-structuring optical chips, which hinders fabrication processes [27]. Accordingly, 1D PhCs present more straightforward designs suitable for mass-level production, while preserving the slow light advantages from compactness [28]. In addition, this type of structures does not need additional periodic cells in the transverse spatial direction, thus reducing the lateral size and the footprint of the device. 1D

This work was supported by Generalitat Valenciana under AVANTI/2019/123 and ACIF/2019/009 grants; by the Spanish Ministerio de Ciencia e Innovación through PID2019-106965RB-C21 and PID2019-111460GB-I00 projects, and by the European Union through the operational program of the European Regional Development Fund (FEDER) of the Valencia Regional Government 2014-2020.

L. Torrijos-Morán, A. Brimont, A. Griol, P. Sanchis and J. García-Rupérez are with the Nanophotonics Technology Center (NTC), Universitat Politècnica de València, Valencia 46022, Spain (e-mail: luitorm2@ntc.upv.es; abrimont@ntc.upv.es; agriol@ntc.upv.es; pabsanki@ntc.upv.es; jaigarru@ntc.upv.es).

This article has been accepted for publication in a future issue of this journal, but has not been fully edited. Content may change prior to final publication. Citation information: DOI 10.1109/JLT.2021.3066479, Journal of Lightwave Technology

PhCs have been demonstrated for tunable delay lines [29], refractometric sensing [30], negative group velocity phenomena [31], slow light engineering waveguides [32] and biosensing [33], among others. Accordingly, high speed electro-optic modulators based on 1D PhCs in MZI configurations have also been demonstrated [34], although the interferometric structure still poses a limit on the minimum achievable footprint. To overcome some of these size limitations, single-channel structures based on bimodal interferometry in periodic subwavelength waveguides are proposed for the development of ultra-sensitive sensors [35], [36]. Furthermore, bimodal 1D PhC waveguides working in the slow light regime have also been designed as ultra-compact modulators with footprints of only 100 μm^2 [37]. In these last structures, the operation is based on the interference between two modes of the same polarization and parity in a single-channel silicon structure, with a large group velocity difference and without the need of additional structures or other materials.

In this paper, we propose the use of bimodal 1D PhC waveguides based on silicon as highly efficient and ultra-compact 2x2 optical switches. We optimize the periodic unit cell of the 1D PhC to support two TE-like modes of both even and odd symmetry, designed with a large group velocity difference. The device is experimentally demonstrated for thermo-optic switching with a very good agreement with simulations. Our design encompasses the benefits from 1D PhCs and bimodal waveguides, to validate this type of structures for optical switching with extremely reduced footprints.

II. Concept and Design

The proposed design of the device is presented in Fig. 1, with a periodic bimodal waveguide acting as the switching structure and four single-mode silicon waveguides acting as input and output ports. The unit cell of the periodic bimodal section is designed to be within the photonic crystal regime and to support the fundamental even mode and a higher order odd mode at the transversal plane, both for the transverse-electric (TE) polarization. Due to symmetry conditions, the fundamental mode of the displaced single-mode input waveguide excites the even and odd parity modes in the bimodal section, which propagate and interfere at the abrupt discontinuity with the single-mode output waveguides. Therefore, the transferred power may be expressed as a function of the phase shift accumulated between these two modes in the bimodal section, thus creating an interference pattern in the transmitted spectra. In addition, a rectangular taper section for an efficient modal excitation is placed at the interface between the access ports and the bimodal waveguide.

In PhC theory, when two modes of the same polarization and parity are expected to intersect, they couple in the same band and form an anti-crossing point [37], [38]. In contrast, modes of different parity do not interact in the band formation, so that they can be overlapped with different dispersion properties. Consequently, using modes of even and odd symmetry provides an additional degree of freedom in obtaining broadband and highly dispersive bimodal regions, since their dispersion relationships can be designed independently by a proper control of the unit cell dimensions. Figure 2(a) shows the first seven bands for a unit cell with pitch $a = 370$ nm, transversal element width $w_i = 220$ nm, transversal element length $w_e = 1700$ nm and central waveguide width $w = 650$ nm, everything in a fully etched silicon layer of 220 nm thickness covered by a silica cladding. The rest of the design parameters considered are single-mode waveguide width $w_s = 450$ nm, taper length $t = 1200$ nm and distance between the ports $d = 300$ nm. To obtain the bands structure of the 1D PhC, definite-frequency eigenstates of Maxwell's equations have been computed by Plane Wave Expansion (PWE) numerical methods using the MIT Photonics Bands (MPB) software [39]. As a result, a bimodal behavior between the third even band and the second odd band is obtained for an operating wavelength around 1550 nm, as depicted by the green shaded area in Fig. 2(a). In this region, the third even and second odd bands are formed by the fundamental and the first higher order odd modes folded into the Brillouin zone. Note that the odd mode presents a slow light behavior at two different wavelengths: at the anti-crossing point with the third odd band and at the end of the first Brillouin zone, both marked with circles in Fig. 2(a) and (b). At these wavelengths, the group index of the odd mode is drastically increased whereas a highly dispersive region with a large bandwidth is obtained in between, as shown in the lower graph in Fig. 2(b). On the other hand, the even mode presents a non-dispersive behavior with low group index values for the entire bimodal region. Therefore, a relatively flat and broad spectral region exhibiting a large group index contrast between the even and odd modes is obtained in the bimodal region.

The electric field distribution of the even and odd modes at the flat region of the group index is shown in Fig. 2(c). The even mode is strongly confined within the central waveguide, while the odd mode interacts with the transversal corrugations, which causes the highly dispersive behavior of this mode. Fully-vectorial 3D Finite-Difference Time-Domain (FDTD) simulations using CST Studio software have been employed to compute the electric field propagation in the optical switch by injecting light into an input waveguide port, as depicted in Fig. 2(d). The complete device with the input and output single-mode waveguides, the tapers and the bimodal periodic structure has been considered to evaluate the switching performance when the silicon refractive index is changed. The full optical switching from the bar to the cross states can be achieved by a bimodal structure of only $N = 100$ periods with a silicon refractive index change of 0.0137.

To optimize the switching performance, the most critical design parameter that determines the effective index contrast between the even and odd modes is the transversal element length of the periodic structure, w_e. By increasing this parameter, the spectral distance between the slow light regions is reduced, thus increasing the group index in the flat region, but at expenses of reducing the optical bandwidth. This fact is due to the influence of such parameter on the cut-off frequency of the higher order odd mode. However, increasing the group index of slow light modes also leads to a reduction of the coupling efficiency that increases the insertion losses, which

This article has been accepted for publication in a future issue of this journal, but has not been fully edited. Content may change prior to final publication. Citation information: DOI 10.1109/JLT.2021.3066479, Journal of Lightwave Technology

must be also considered. Additionally, insertion losses are also due to the field distribution mismatch between the fundamental mode of the in-output waveguide and the higher order mode of the PhC. Figure 3(a) shows the trade-off between the group index obtained for the odd mode and the insertion losses, both in the flat region. Note that these values remain around 2 dB up to a w_e of 1700 nm, from which the design becomes highly lossy as the group index increases. Therefore, the design presents high tolerances to fabrication deviations regarding w_e. Two different designs of $w_{e1} = 1600$ nm and $w_{e2} = 1700$ nm with odd mode group indices of 7.85 and 9.14, respectively, have been considered for changes in the silicon refractive index. In bimodal waveguides, since both modes interact with variations in the material optical properties, the length required to obtain a phase shift of π for a given change in refractive index is mathematically expressed as

$$L_\pi = \frac{\lambda}{2\left(\Delta n_{eff,o} - \Delta n_{eff,e}\right)} \quad (1)$$

where λ is the wavelength, and $\Delta n_{eff,o}$ and $\Delta n_{eff,e}$ is the change in the effective index of the odd and even modes, respectively. Figure 3(b) depicts the π lengths obtained for different silicon refractive index changes at a wavelength of 1560 nm, which is within the flat region of group index. Both w_{e1} and w_{e2} designs of the bimodal 1D PhC have been computed, as well as for a conventional homogeneous single-mode waveguide of 450 nm width and 220 nm thickness. The length obtained in the 1D PhC waveguides is shorter than in the homogeneous waveguide, even though in the bimodal case the resulting effective index change is the difference between the two modes contribution. In addition, the length obtained in the w_{e2} design is clearly shorter than in the w_{e1} case, due to the higher group index obtained for the first configuration. As a result, compact footprints can be achieved in the w_{e2} design since the interferometry is produced in a single-channel waveguide and very short lengths are needed. Specifically, two lengths of 37 μm and 74 μm, corresponding to 100 and 200 periods, are considered for the experimental evaluation for the w_{e2} and w_{e1} configurations, respectively.

III. Fabrication and Characterization of the Chip

The two w_{e1} and the w_{e2} bimodal PhC designs with their respective lengths previously determined have been fabricated on a silicon-on-insulator platform with a silicon layer thickness of 220 nm and a silica buried layer of 2 μm. Regarding the fabrication process, 30 KeV of acceleration voltage and 30 μm of aperture size have been employed in the electron-beam lithography process to expose the photonic structures on a hydrogen silsesquioxane (HSQ) negative resist. Likewise, inductively plasma etching has been used to transfer the photonic designs onto the silicon layer. Finally, a silica cover layer of 700 nm has been deposited on the sample, on which a lift-off process has been used to evaporate titanium heaters of 160 nm thickness over the 1D PhC structures. The heaters dimensions are 37 μm x 4 μm in the short w_{e2} design and 74 μm x 4 μm in the long w_{e2} design. The dimensions of the titanium pads are 100 μm x 100 μm in both configurations, with a separation between them of 200 μm.

Figure 4(a) shows the optical microscope images of the fabricated chip with both w_{e1} and w_{e2} designs, and their corresponding heaters. A scanning electron microscope (SEM) image of the entire fabricated switching structure of $N = 200$ periods and w_{e1} is shown in Fig. 4(b) and a detailed image of the bimodal 1D PhC waveguide is shown in Fig. 4(c). For the optical characterization, a continuous wave laser (Keysight 81980) with a TE polarizer was employed to inject light into the chip by using on-chip grating couplers. A synchronized power meter (Keysight 81636B) at the output, controlled by a LabVIEW application, was used to record the transmitted spectra.

IV. Experimental Demonstration

The normalized transmitted spectra for the bar and cross states are depicted for both w_{e1} and w_{e2} configurations in Fig. 5. As it is shown, an interference pattern is experimentally obtained as a result of the constructive and destructive interferences between the even and odd modes in the bimodal 1D PhC. The number of spectral peaks available in Fig. 5(a) is higher than in Fig. 5(b) due to the increment in the physical length in the first case. It should be also noted that the modal excitation is decreased for those wavelengths near the slow light regions predicted in Fig. 2(b), while the coupling efficiency is improved in between. In this region, experimental insertion losses around 1.9 dB and extinction ratios higher than 17 dB are observed for w_{e1} and w_{e2} configurations at a wavelength of 1576 nm and 1590 nm, respectively, which is in a good agreement with the simulations. For these wavelengths, a crosstalk of 15 dB between bar and cross states is measured with a bandwidth of 0.5 nm and 1 nm for w_{e1} and w_{e2} configurations, respectively.

To determine the dispersive behavior of the bimodal 1D PhC [18], the experimental group index of the higher order odd mode is calculated from the bimodal oscillations in the transmitted spectra by using the following equation:

$$n_g^o(\lambda) = \frac{\lambda_{\max}\lambda_{\min}}{2L\left(\lambda_{\max} - \lambda_{\min}\right)} + n_g^e(\lambda) \quad (2)$$

where λ_{max} is the maxima and λ_{min} the minima positions of the transmission bimodal oscillations, L the length of the bimodal region and n_g^e is the simulated group index of the even mode as a function of wavelength. In Fig. 5(a) and (b) the positions of the maxima and minima are marked with circles for the bar port transmitted spectrum. The resulting experimental group index obtained is depicted in Fig. 5(c), as well as the fitting curve and the simulated even mode group index. These experimental measurements match the theoretical results in Fig. 2(b), regarding the definition of two slow light zones of extremely large group index contrast. Between these two zones, a flat region of almost a constant group index for the odd mode is obtained. A specific group index value of 7.6 and 9 at the wavelengths previously considered is experimentally obtained for the w_{e1} and w_{e2} configurations, respectively, which perfectly match the simulations in Fig. 3(a). Moreover, the optical bandwidth of the group index flat region is reduced because of the influence of the w_{e2} dimension in the band structure formation, as it was theoretically predicted. A large group index contrast flat region of 45 nm and 33 nm is

experimentally measured for the w_{e1} and w_{e2} designs, respectively.

To validate the device as an optical switch, the transmitted spectra in the bar and cross states have been recorded when applying an electrical signal to the titanium heaters. Due to the thermo-optic coefficient of silicon, the optical response is tuned by the temperature changes in the structure caused by the heaters. Figure 6(a) and (b) shows the optical response in the bar and cross states of the w_{e1} and w_{e2} switches, respectively, for different voltages. The results present a positive spectral shift originated by an increment in the temperature, which corresponds to a phase shift around π for both designs. To determine the power consumption of the switch, the spectral dips previously detailed at 1576 nm and 1590 nm have been considered in the w_{e1} and w_{e2} designs, respectively. The phase shift accumulated in the bimodal waveguide may be obtained from the transmitted spectra as:

$$\Delta\varphi(\lambda) = \frac{2\Delta\lambda}{\left(FSR_H + FSR_L\right)} \tag{3}$$

where $\Delta\lambda$ is the spectral shift of the transmission dip, and $FSR_{H,L}$ are the free spectral range between consecutive dips at higher and lower wavelengths, respectively. In the left graph of Fig. 6(c), the estimated phase shift with Eq. (3) is depicted as a function of the applied electrical power. As it was previously predicted, the w_{e2} design presents a higher switching efficiency than the w_{e1} design, as a result of the higher odd mode group index for this configuration. Concretely, a power consumption of 19.5 mW is demonstrated in the w_{e2} configuration, whereas 24.5 mW is obtained in the w_{e1} configuration, for a π-phase shift. The right graph of Fig. 6(c) depicts the optical power of the bar and cross states versus the applied electrical power, for both wavelengths previously considered within the flat region of the group index. It is shown that a lower electrical power is needed in the w_{e2} design to switch from a minimum optical peak to a maximum. Consequently, a higher power consumption is required in the w_{e1} design, which confirms the higher efficiency obtained for the w_{e2} configuration.

V. Conclusion

To conclude, we have demonstrated an ultra-compact electro-optical 2x2 switch based on a slow-light-enhanced bimodal waveguide and driven by the thermo-optic effect in silicon. In contrast to other similar work [37], the periodic unit cell is designed to support two modes of both even and odd symmetries in the bimodal part of the band structure. We benefit from this fact to engineer a broadband region of large group index contrast, thereby improving the switching performance. Two different designs have been considered to show the trade-off between the group index contrast and the insertion losses. In comparison with the literature, simulations have demonstrated a higher efficiency for both slow-light-enhanced bimodal configurations compared to a standard silicon waveguide integrated in ring resonators and MZI-based switches [3], [4], [6]. Moreover, the interferometry has been carried out in a single-channel structure without the need of additional photonic elements, which have significantly reduced the final size of the device. As a result, an ultra-compact switch with a footprint of only 63 μm^2 was achieved, which is smaller than the ones reported in related PhC-based works in MZI configurations [17], [21] and similar to the ones observed in 2D PhC [22]–[25], but in our case in a straightforward design that eases the fabrication processes and cost for high-level production. An insertion loss of 1.8 dB and a crosstalk of 15 dB over a 1 nm bandwidth were obtained with a power consumption of 19.5 mW. The resulting bandwidth is smaller than for conventional MZI switches [7] but higher than in the case of RR switches [5]. On the other hand, insertion losses is higher than in conventional MZIs or ring resonators, where values below 0.5 dB have been reported by using thermo-optic phase shifters [40], [41]. However, the taper geometry could be further optimized to minimize insertion losses [42], while power consumption could also be reduced with an improved design of the heaters [11]. The results suggest the use of these types of structures in photonic switching for datacenters in which large matrices are not required and the overall photonic integrated circuit size would be drastically reduced [43]. Furthermore, future work in lowering losses would be highly desirable for improving scalability and addressing other potential applications such as LIDAR systems, programmable circuits, or neuromorphic computing.

References

[1] D. Thomson *et al.*, "Roadmap on silicon photonics," *J. Opt.*, vol. 18, no. 7, 2016.

[2] H. Subbaraman *et al.*, "Recent advances in silicon-based passive and active optical interconnects," *Opt. Express*, vol. 23, no. 3, p. 2487, 2015.

[3] D. Nikolova *et al.*, "Scaling silicon photonic switch fabrics for data center interconnection networks," *Opt. Express*, vol. 23, no. 2, p. 1159, 2015.

[4] P. Dong, S. F. Preble, and M. Lipson, "All-optical compact silicon comb switch," *Opt. Express*, vol. 15, no. 15, p. 9600, 2007.

[5] A. Biberman *et al.*, "Broadband silicon photonic electrooptic switch for photonic interconnection networks," *IEEE Photonics Technol. Lett.*, vol. 23, no. 8, pp. 504–506, 2011.

[6] A. Densmore *et al.*, "Compact and low power thermo-optic switch using folded silicon waveguides," *Opt. Express*, vol. 17, no. 13, p. 10457, 2009.

[7] J. Van Campenhout, W. M. Green, S. Assefa, and Y. A. Vlasov, "Low-power, 2×2 silicon electro-optic switch with 110-nm bandwidth for broadband reconfigurable optical networks," *Opt. Express*, vol. 17, no. 26, p. 24020, 2009.

[8] M. R. Watts, J. Sun, C. Derose, D. C. Trotter, R. W. Young, and G. N. Nielson, "Adiabatic thermo-optic Mach – Zehnder switch," *Opt. Lett.*, vol. 38, no. 5, pp. 733–735, 2013.

[9] F. Wang, J. Yang, L. Chen, X. Jiang, and M. Wang, "Optical switch based on multimode interference coupler," *IEEE Photonics Technol. Lett.*, vol. 18, no. 2, pp. 421–423, 2006.

[10] Á. Rosa, A. Gutiérrez, A. Brimont, A. Griol, and P. Sanchis, "High performace silicon 2x2 optical switch based on a thermo-optically tunable multimode interference coupler and efficient electrodes," *Opt. Express*, vol. 24, no. 1, p. 191, 2016.

[11] J. Parra, J. Hurtado, A. Griol, and P. Sanchis, "Ultra-low loss hybrid ITO/Si thermo-optic phase shifter with optimized power consumption," *Opt. Express*, vol. 28, no. 7, p. 9393, 2020.

[12] R. Amin *et al.*, "0.52 v mm ITO-based Mach-Zehnder modulator in silicon photonics," *APL Photonics*, vol. 3, no. 12, pp. 0–11, 2018.

[13] E. Li, B. A. Nia, B. Zhou, and A. X. Wang, "Transparent conductive oxide-gated silicon microring with extreme resonance wavelength tunability," *Photonics Res.*, vol. 7, no. 4, p. 473, 2019.

[14] R. Amin *et al.*, "Sub-wavelength GHz-fast broadband ITO Mach–Zehnder modulator on silicon photonics," *Optica*, vol. 7, no. 4, p. 333, 2020.

[15] S. Campione *et al.*, "Submicrometer Epsilon-Near-Zero Electroabsorption Modulators Enabled by High-Mobility Cadmium Oxide," *IEEE Photonics J.*, vol. 9, no. 4, 2017.

[16] J. Parra, I. Olivares, F. Ramos, and P. Sanchis, "Ultra-compact non-volatile Mach–Zehnder switch enabled by a high-mobility transparent conducting oxide," *Opt. Lett.*, vol. 45, no. 6, p. 1503, 2020.
[17] E. A. Camargo, H. M. H. Chong, and R. M. De La Rue, "2D Photonic crystal thermo-optic switch based on AlGaAs/GaAs epitaxial structure," *Opt. Express*, vol. 12, no. 4, p. 588, 2004.
[18] Y. A. Vlasov, M. O'Boyle, H. F. Hamann, and S. J. McNab, "Active control of slow light on a chip with photonic crystal waveguides," *Nature*, vol. 438, no. 7064, pp. 65–69, 2005.
[19] T. F. Krauss, "Slow light in photonic crystal waveguides," *J. Phys. D. Appl. Phys.*, vol. 40, no. 9, pp. 2666–2670, 2007.
[20] T. Baba, "Slow light in photonic crystals," *Nat. Photonics*, vol. 2, no. 8, pp. 465–473, 2008.
[21] H. Nakamura, Y. Sugimoto, K. Kanamoto, and N. Ikeda, "Ultra-fast photonic crystal/quantum dot all-optical switch for future photonic networks," *Opt. Express*, vol. 12, no. 26, pp. 6606–6614, 2004.
[22] Z. Li, Y. Zhang, and B. Li, "Terahertz photonic crystal switch in silicon based on self-imaging principle," *Opt. Express*, vol. 14, no. 9, p. 3887, 2006.
[23] N. Yamamoto, T. Ogawa, and K. Komori, "Photonic crystal directional coupler switch with small switching length and wide bandwidth," *Opt. Express*, vol. 14, no. 3, p. 1223, 2006.
[24] D. M. Beggs, T. P. White, L. O'Faolain, and T. F. Krauss, "Ultracompact and low-power optical switch based on silicon photonic crystals," *Opt. Lett.*, vol. 33, no. 2, p. 147, 2008.
[25] K. Nozaki *et al.*, "Sub-femtojoule all-optical switching using a photonic-crystal nanocavity," *Nat. Photonics*, vol. 4, no. 7, pp. 477–483, 2010.
[26] Y. A. Vlasov and S. J. McNab, "Coupling into the slow light mode in slab-type photonic crystal waveguides," *Opt. Lett.*, vol. 31, no. 1, p. 50, 2006.
[27] M. Notomi, "Manipulating light with strongly modulated photonic crystals," *Reports Prog. Phys.*, vol. 73, no. 9, 2010.
[28] M. Centini *et al.*, "Dispersive properties of finite, one-dimensional photonic band gap structures: Applications to nonlinear quadratic interactions," *Phys. Rev. E*, vol. 60, no. 4, pp. 4891–4898, 1999.
[29] M. Scalora *et al.*, "Ultrashort pulse propagation at the photonic band edge: Large tunable group delay with minimal distortion and loss," *Phys. Rev. E*, vol. 54, no. 2, pp. 1078–1081, 1996.
[30] W. C. L. Hopman *et al*., "Quasi-one-dimensional photonic crystal as a compact building-block for refractometric optical sensors," *IEEE J. Sel. Top. Quantum Electron.*, vol. 11, no. 1, pp. 11–15, 2005.
[31] R. B. Hwang, "Negative group velocity and anomalous transmission in a one-dimensionally periodic waveguide," *IEEE Trans. Antennas Propag.*, vol. 54, no. 2, pp. 755–760, 2006.
[32] A. Brimont, A. Griol, J. Martí, P. Sanchis, J. Mart??, and P. Sanchis, "Group index engineering in silicon corrugated waveguides," *IEEE Int. Conf. Gr. IV Photonics GFP*, vol. 35, no. 16, pp. 39–41, 2010.
[33] J. Sabek *et al.*, "Experimental study of an evanescent-field biosensor based on 1D photonic bandgap structures," *Beilstein J. Nanotechnol.*, vol. 10, pp. 967–974, 2019.
[34] A. Brimont *et al*., "High speed silicon electro-optical modulators enhanced via slow light propagation," *Opt. Express*, vol. 19, no. 21, p. 20876, 2011.
[35] L. Torrijos-Morán and J. García-Rupérez, "Single-channel bimodal interferometric sensor using subwavelength structures," *Opt. Express*, vol. 27, no. 6, pp. 8168–8179, 2019.
[36] L. Torrijos-Morán, A. Griol, and J. García-Rupérez, "Experimental study of subwavelength grating bimodal waveguides as ultrasensitive interferometric sensors," *Opt. Lett.*, vol. 44, no. 1, pp. 4702–4705, 2019.
[37] L. Torrijos-Morán, A. Griol, and J. García-Rupérez, "Slow light bimodal interferometry in one- dimensional photonic crystal waveguides," *Light Sci. Appl.*, vol. 10, no. 16, 2021.
[38] M. Notomi, K. Yamada, A. Shinya, J. Takahashi, C. Takahashi, and I. Yokohama, "Extremely large group-velocity dispersion of line-defect waveguides in photonic crystal slabs," *Phys. Rev. Lett.*, vol. 87, no. 25, pp. 253902-253902–4, 2001.
[39] S. Johnson and J. Joannopoulos, "Block-iterative frequency-domain methods for Maxwell's equations in a planewave basis," *Opt. Express*, vol. 8, no. 3, pp. 173–190, 2001.
[40] Q. Fang *et al.*, "Ultralow power silicon photonics thermo-optic switch with suspended phase arms," *IEEE Photonics Technol. Lett.*, vol. 23, no. 8, pp. 525–527, 2011.
[41] N. Sherwood-Droz *et al.*, "Optical 4x4 hitless Silicon router for optical Networks-on-Chip (NoC): erratum," *Opt. Express*, vol. 16, no. 23, p. 19395, 2008.
[42] X. Zhao, H. Dalir, X. Xu, and R. T. Chen, "Efficient coupling into slow-light one-dimensional fishbone waveguide by mode converter method," *Appl. Phys. Express*, vol. 10, no. 7, 2017.
[43] Q. Cheng, S. Rumley, M. Bahadori, and K. Bergman, "Photonic switching in high performance datacenters [Invited]," *Opt. Express*, vol. 26, no. 12, p. 16022, 2018.

Luis Torrijos-Morán was born in Valencia, Spain, in 1991. He received the B.S. degree in telecommunication and the M.S. degree in electronics engineering from the Universitat de València, Spain, in 2015 and 2016, respectively. He is currently pursuing the Ph.D. degree in telecommunications with the Universitat Politècnica de València (UPV), Spain. Since 2016, he has been a Research Assistant with the Biophotonics Research Group, Nanophotonics Technology Center, UPV. His research interests include the development of photonic devices, including optical interferometers, photonic crystals, and bimodal waveguides.

Antoine Brimont was born in Valence, France, in 1982. He received the Engineering Master's degree in materials science and nanotechnology from the Institut National des Sciences Appliquees de Rennes, Rennes, France, as well as the M.Sc. degree in physics in collaboration with the University of Rennes, Rennes, France, in 2005. He also received the Ph.D. degree in telecommunications engineering from the Polytechnic University of Valencia, Valencia, Spain, in 2011. He is currently a Senior Research Engineer at the Valencia Nanophotonics Technology Center, Polytechnic University of Valencia. His research interests include integrated silicon photonics and specifically high-speed silicon modulators. He has authored or co-authored more than 40 papers in peer-reviewed international journals and international conferences.

Amadeu Griol was born in Valencia, Spain, in 1973. He received the Telecommunication Engineer and Ph.D. degrees from the Universitat Politècnica de València in 1998 and 2003, respectively. His research interests include fabrication, modeling, and characterization of electrical and optical devices, especially microwave microstrip filters with harmonic suppression techniques and also photonic integrated circuits and nanophotonic devices for communication as well as biosensing applications. He has been working for more than ten years in the fabrication of optical micro- and nanodevices by using electron beam lithography techniques. He has been involved in several FP6, FP7, and H2020 European projects in charge of optical devices micro- and nanofabrication tasks. He authored and coauthored more than 50 papers in international journals, more than 100 contributions to international conferences and 2 patents.

Pablo Sanchis received the PhD degree from the Universitat Politècnica in 2005. He is Full-Professor at the same university since 2016. His research career has been developed at the Nanophotonics Technology Center where he leads a research group. His research interests are basically related with the design, fabrication and characterization of photonic integrated circuits, especially in the field of silicon photonics. He has

This article has been accepted for publication in a future issue of this journal, but has not been fully edited. Content may change prior to final publication. Citation information: DOI 10.1109/JLT.2021.3066479, Journal of Lightwave Technology

authored more than 80 papers in peer-reviewed international journals and more than 140 papers in international conferences and he holds several patents. He has also been part of the organization committee of ECOC, ECIO, and other international conferences.

Jaime García-Rupérez (M'03–SM'16) received the M.S. and Ph.D. degrees in telecommunication from the Universitat Politècnica de València, Spain, in 2002 and 2008, respectively. He is Associate Professor in the Universitat Politècnica de València and Leader of the Biophotonics Research Group from the Nanophotonics Technology Centre. His work focuses on the development of integrated photonic biosensing systems for its application in fields as medical diagnosis, environmental control or biological safety. Dr. García-Rupérez has authored over 150 journal and conference publications, one book chapter, and five patents.

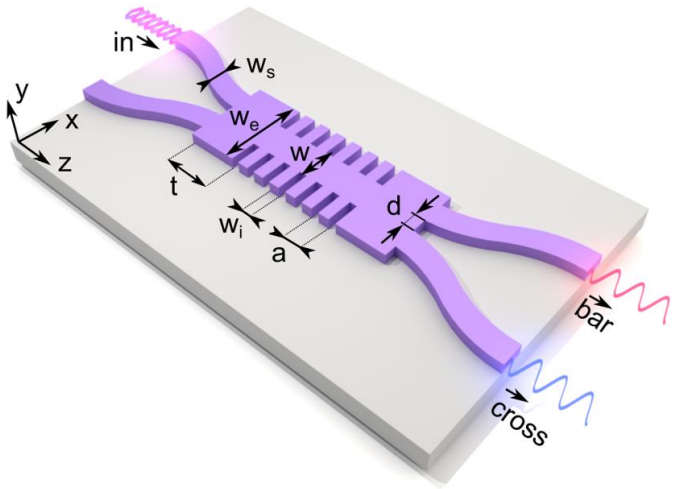

Fig. 1. Device schematic of the proposed 2x2 optical switch design, composed of two input and output single-mode silicon waveguides, a bimodal 1D PhC structure and a rectangular taper or transition between these two parts, placed both at the input and output interfaces.

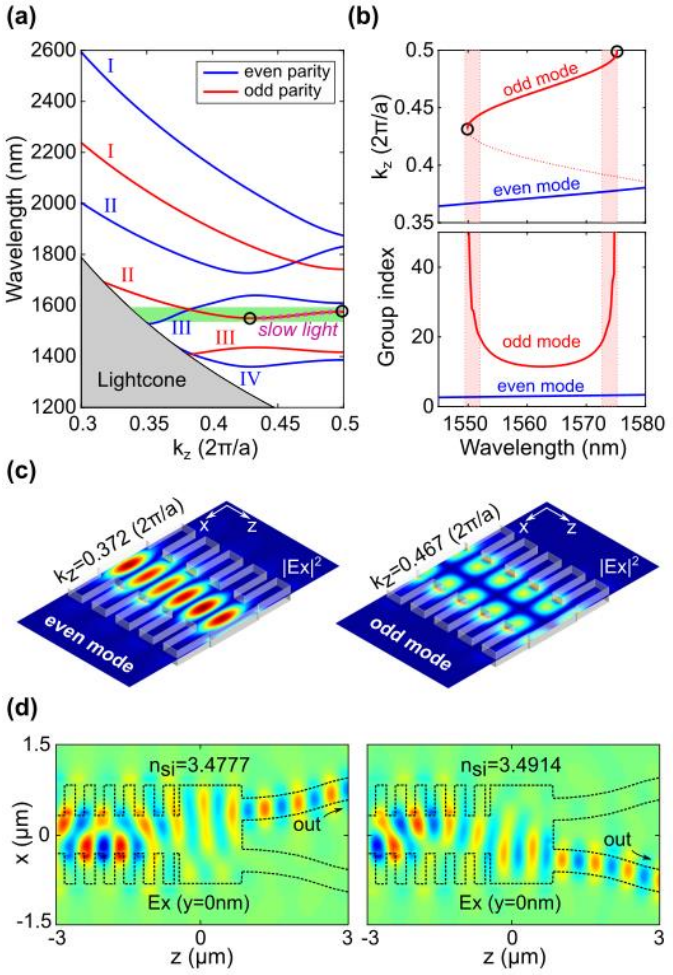

Fig. 2. (a) Band structure of the 1D PhC periodic unit cell for the TE-like polarized bands. The dimensions considered for the simulations are $a = 370$ nm, $w_i = 220$ nm, $w_e = 1700$ nm, $w = 650$ nm and $w_s = 450$ nm, with a height of 220 nm. The roman numerals indicate the band formation order for the even and odd parity bands. The green shaded area indicates the bimodal region of interest, where the odd parity band becomes slow light. Circles mark the region where the group velocity of the band is critically reduced. (b) Detailed band structure and group index for both even and odd modes in the bimodal region, upper and lower graph, respectively. (c) Absolute value of the electric field x-component at $y = 0$ nm plane for the third even parity band and the second odd

This article has been accepted for publication in a future issue of this journal, but has not been fully edited. Content may change prior to final publication. Citation information: DOI 10.1109/JLT.2021.3066479, Journal of Lightwave Technology

parity band, both at the bimodal region at 1564 nm. (d) 3D-FDTD simulation of the real part x-component electric field propagation at $y = 0$ nm plane when the silicon refractive index changes at 1556 nm wavelength.

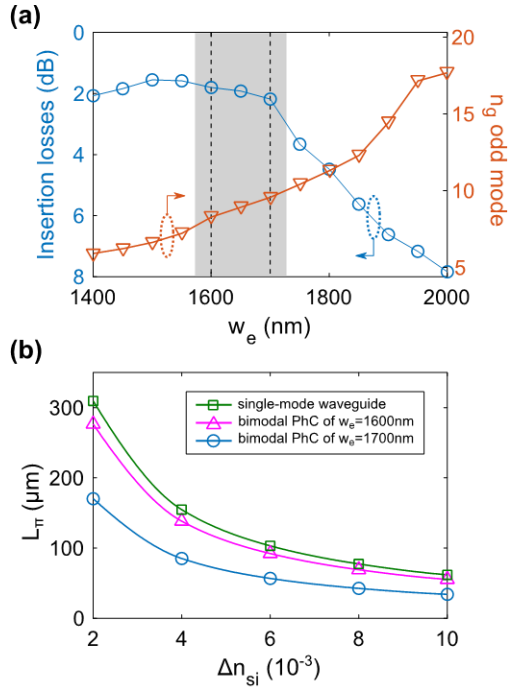

Fig. 3. (a) Trade-off between the insertion losses and the group index of the odd parity mode as a function of the transversal element width w_e. The rest of the design parameters are the same previously considered. (b) Simulated π length for different silicon refractive index increments at a common wavelength of 1560 nm.

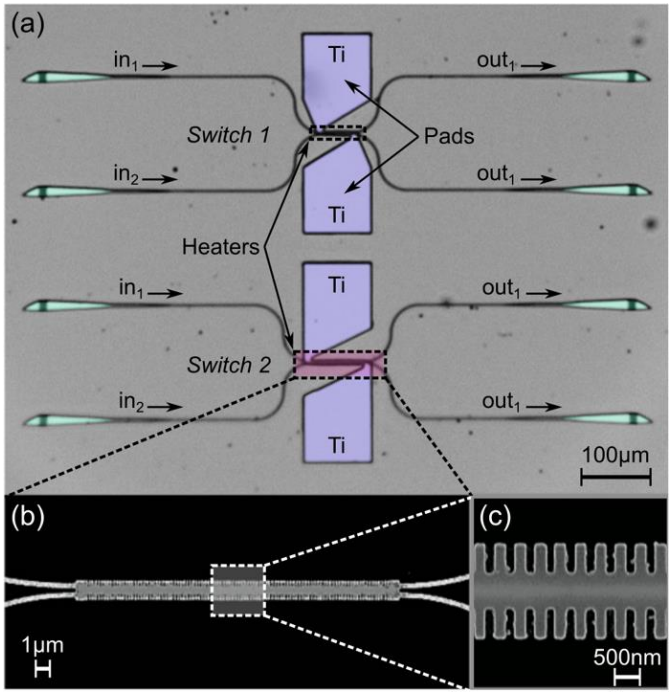

Fig. 4. (a) Optical microscope image of the fabricated chip with the input and output grating couplers, the titanium (Ti) heaters and lateral pads. Upper and lower switches have a length of 37 μm and 74 μm for w_{e2} and w_{e1} designs, respectively. (b) SEM image of the optical switch of $N = 200$ periods and $w_e = 1600$ nm with the input and output single mode waveguides and (c) detailed 1D PhC structure in silicon.

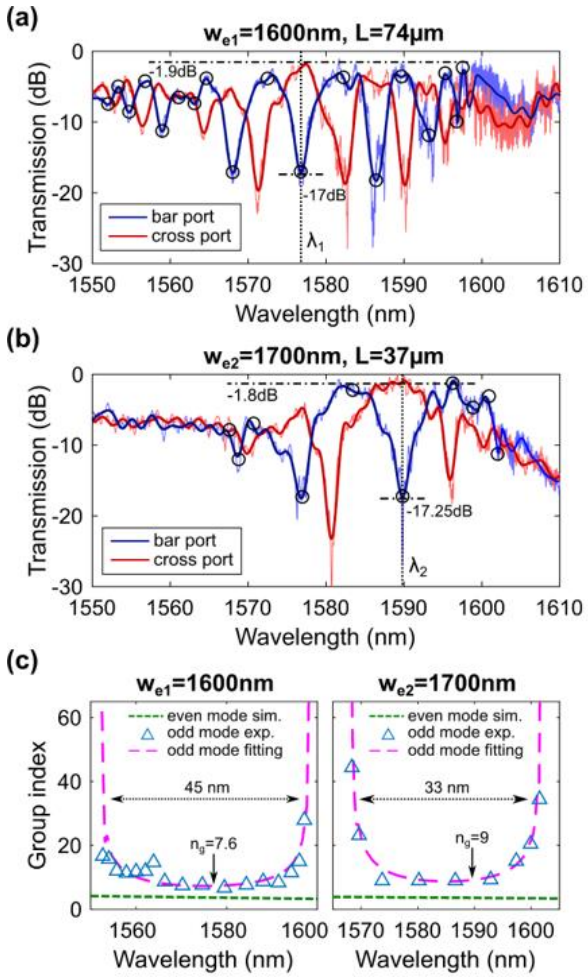

Fig. 5. Normalized transmission spectra of the fabricated optical 2x2 switches with a transversal element width (a) w_{e1} and (b) w_{e2} with a silica cover as upper cladding. The normalization has been calculated respect to a reference waveguide of the same length. The filtered spectra are shown over the raw experimental data, in dark and light colors, respectively. Maxima and minima peaks corresponding to the constructive and destructive interferences are marked with circles. (c) Experimental group index calculated from the spectra minima and maxima peaks as a function of wavelength for both w_{e1} and w_{e2} designs.

This article has been accepted for publication in a future issue of this journal, but has not been fully edited. Content may change prior to final publication. Citation information: DOI 10.1109/JLT.2021.3066479, Journal of Lightwave Technology

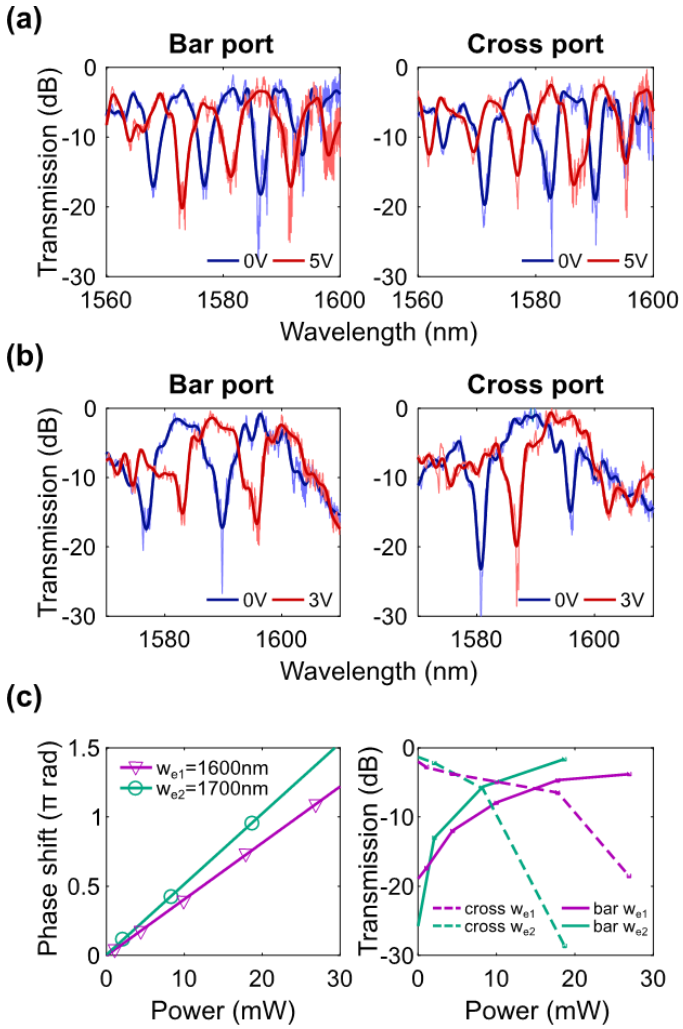

Fig. 6. Normalized transmission spectra for different voltages and for both designs of (a) $w_{e1} = 1600$ nm with a device length of 74 µm and (b) $w_{e2} = 1700$ nm with a device length of 37 µm. (c) Phase shift and optical power as a function of the electrical power applied, left and right graph, respectively. A wavelength of 1576 nm and 1590 nm have been considered for the w_{e1} and w_{e2} designs, respectively, both in the flat region of the group index.